CrossMark

J. Fluid Mech. (2017), *vol.* 817, *pp.* 61–79. © Cambridge University Press 2017
doi:10.1017/jfm.2017.110

On the normalized dissipation parameter C_ϵ in decaying turbulence

L. Djenidi[1,†], N. Lefeuvre[1], M. Kamruzzaman[1] and R. A. Antonia[1]

[1]Discipline of Mechanical Engineering, School of Engineering, University of Newcastle, Newcastle, 2308 NSW, Australia

(Received 22 August 2016; revised 10 February 2017; accepted 10 February 2017; first published online 15 March 2017)

The Reynolds number dependence of the non-dimensional mean turbulent kinetic energy dissipation rate $C_\epsilon = \overline{\epsilon}L/u'^3$ (where ϵ is the mean turbulent kinetic energy dissipation rate, L is an integral length scale and u' is the velocity root-mean-square) is investigated in decaying turbulence. Expressions for C_ϵ in homogeneous isotropic turbulent (HIT), as approximated by grid turbulence, and in local HIT, as on the axis of the far field of a turbulent round jet, are developed from the Navier–Stokes equations within the framework of a scale-by-scale energy budget. The analysis shows that when turbulence decays/evolves in compliance with self-preservation (SP), C_ϵ remains constant for a given flow condition, e.g. a given initial Reynolds number. Measurements in grid turbulence, which does not satisfy SP, and on the axis in the far field of a round jet, which does comply with SP, show that C_ϵ decreases in the former case and remains constant in the latter, thus supporting the theoretical results. Further, while C_ϵ can remain constant during the decay for a given initial Reynolds number, both the theory and measurements show that it decreases towards a constant, $C_{\epsilon,\infty}$, as Re_λ increases. This trend, in agreement with existing data, is not inconsistent with the possibility that C_ϵ tends to a universal constant.

Key words: homogeneous turbulence, isotropic turbulence, turbulence theory

1. Introduction

It is commonly believed that the constancy of the non-dimensional dissipation rate parameter $C_\epsilon = \overline{\epsilon}L/u'^3$ (where $\overline{\epsilon}$ is the dissipation rate of the mean turbulent kinetic energy, C_ϵ is the dissipation coefficient and constant, u' is the velocity root-mean-square and L an integral length scale; the overbar represents time average) is a cornerstone assumption of turbulence, e.g. Tennekes & Lumley (1972), McComb *et al.* (2015), Vassilicos (2015); see also McComb (2014) for a brief review. It is often interpreted as representing the transfer of energy from larger to smaller scales of motion (Tennekes & Lumley 1972). Interestingly, this interpretation was not made by Taylor (1935) who first introduced this constant. In fact, it is his attempt to connect $\overline{\epsilon}$ to the velocity correlation function that led him to this dissipation scaling. Since the focus of this study is on C_ϵ, it is worthwhile reproducing Taylor's introduction of C_ϵ. He wrote:

† Email address for correspondence: lyazid.djenidi@newcastle.edu.au

https://doi.org/10.1017/jfm.2017.110 Published online by Cambridge University Press

It has been shown by von Kármán that if the surface stress in a pipe is expressed in the form $\tau = \rho v_x^2$ then

$$\frac{U_c - U}{v_x} = f(r/a), \tag{1.1}$$

where U_c is the maximum velocity in the middle of the pipe and U is the velocity at radius r. This relationship is associated with the conception that the Reynolds stresses are proportional to the squares of the turbulent component of velocity. It seems that the rate of dissipation of energy in such a system must be proportional, so far as changes in linear dimension, velocity and density are concerned, to $\rho u'^3/l$, where l is some linear dimension defining the scale of the system. For turbulence produced by geometrically similar boundaries therefore

$$\overline{\epsilon} = \text{const.} \left(\frac{\rho u'^3}{l}\right) = 15\frac{\nu u'^2}{\lambda^2}. \tag{1.2}$$

For such systems therefore

$$\frac{\lambda^2}{l^2} = C\left(\frac{\nu}{lu'}\right), \tag{1.3}$$

where C depends on the positions relative to the solid boundaries of the point at which observations are made and on the element used for defining l.

Here, ρ is the fluid density, λ is the Taylor microscale, τ is the shear stress and vx is a scaling velocity. For convenience we identify the constant in (1.2) as C_T. Note also that there is some ambiguity about l, which is not necessarily the integral length scale L, although it should characterize the large-scale motion. A few remarks can be made. First, equation (1.2) leads immediately to $C_T = (15/Re_l)l^2/\lambda^2$, where $Re_l = lu'/\nu$ is a scaling Reynolds number. Clearly, since C_T is constant, then $l/\lambda \sim \sqrt{Re_l}$. Second, Taylor uses dimensional arguments for stating that $\overline{\epsilon} \sim \rho u'^3/l$. Third, he uses the local isotropy assumption as is evident from the last term on the right in (1.2). Fourth, the constant $C = (15/C_T)$ may depend on the initial and boundary conditions. Fifth, the statement referring to the Reynolds stresses and expression (1.1) indicates that Taylor assumes the turbulent flow to be in self-preservation (hereafter denoted SP). The hypothesis of SP development of a turbulent flow assumes that all aspects of motion have similar forms at all stages, the differences being described by changes of velocity and length scales which are functions of time (in decaying turbulence) or of position in the flow direction (Townsend 1976); in other words, all mean turbulent quantities are expressible non-dimensionally through suitable scales of length and velocity, and the forms of the normalized distributions remain unchanged at all stages of the flow evolution. Thus, Taylor introduced the constant C_T under the condition that the flow is in SP and isotropy is satisfied. Interestingly, no reference to the Reynolds number is made by Taylor.

Kolmogorov (1941*b*) showed that $\overline{\epsilon} = Ck^{3/2}/L$ (k is the turbulent kinetic energy) with $C = (2g/C_K)^{2/3}$, not necessarily the same as in (1.2), where g is supposed to be a constant and C_K the Kolmogorov constant (defined in $\overline{(\delta u)^2} = C_K(\overline{\epsilon} r)^{2/3}$, δu is the velocity increment and r is the spatial increment). Here, L is related to the

https://doi.org/10.1017/jfm.2017.110 Published online by Cambridge University Press

Loitsiansky length scale Λ as $L = (\Lambda/k)^{1/5}$. Kolmogorov developed the expression of C_ϵ for separations in the range $\lambda \ll r \ll L$ and by assuming SP for $\overline{(\delta u)^2}$, i.e. $\overline{(\delta u)^2} = k\psi(r/L)$, ψ is a dimensionless function of r/L. Clearly, Kolmogorov used L as a SP scaling variable. It is evident that he assumed the existence of an inertial range, which suggests that he assumed a very, if not infinitely, large Reynolds number.

It is interesting to note that both Taylor and Kolmogorov required some form of SP in their respective approaches to obtain C_ϵ, suggesting that the constancy of C_ϵ too requires some form of SP. Accordingly, testing the constancy of C_ϵ, as defined by both Taylor and Kolmogorov, requires that SP should be closely approximated. However, since the work of Taylor and Kolmogorov, the reference to the SP requirement for obtaining C_ϵ appears to have been largely ignored (with some exceptions, e.g. Antonia, Satyaprakash & Hussain (1980)) and the focus has been almost invariably on the dimensional arguments (e.g. Batchelor 1953; Tennekes & Lumley 1972; Sreenivasan 1984; Monin & Yaglom 2007). This has led to testing the constancy of C_ϵ in many turbulent flows which do not necessarily comply with SP, as originally assumed by Taylor and Kolmogorov, such as grid turbulence (Djenidi, Kamruzzaman & Antonia 2015; Sinhuber, Bodenschatz & Bewley 2015). For example, Batchelor (1953) presented values of C_ϵ for grid turbulence at several Reynolds numbers. Despite the scatter in the data, the trend is clear: C_ϵ shows a systematic, albeit weak, decrease with increasing downstream distance and increasing Reynolds number. The Reynolds number dependence was further confirmed by Sreenivasan (1984), who showed that C_ϵ varies strongly when $0 \leqslant Re_\lambda \leqslant 50$, but becomes constant with a value of approximately 1 when $Re_\lambda \geqslant 50$. Recently Vassilicos (2015) presented a review of C_ϵ over the past 60 years and discussed its non-universality. He further proposed, on empirical grounds, that for decaying turbulence, such as wake and grid turbulence, $C_\epsilon \sim Re_I^m/Re_L^n$ with $m \simeq n \simeq 1$ where $Re_I = Ul_b/\nu$ is a global or inlet Reynolds number characterizing the inlet condition (l_b is a length scale defined by the grid e.g. the grid mesh size M).

While dimensional analysis has proven to be quite useful, it lacks the rigour of an analysis based on the equations of motion. Only a very few analyses of C_ϵ were carried out within the framework of the Navier–Stokes equations. Lohse (1994) was probably first to transcend dimensional analysis. He used a mean field theory closure of the Kármán–Howarth equation and obtained $C_\epsilon = C_{\epsilon,\infty}\sqrt{1+\alpha/Re_\lambda^2}$, where $C_{\epsilon,\infty}$ is the value of C_ϵ as $Re_\lambda \to \infty$ and α a constant. He ignored the term accounting for the large-scale motions in the Kármán–Howarth equation. Using the Navier–Stokes equations, Doering & Foias (2002) established the following expression $C_\epsilon \leqslant (a/Re_l + b)$ (a and b are constants independent of the Reynolds number) or equivalently $C_\epsilon \leqslant (b/2)(1 + \sqrt{1+(4a/b^2)/Re_\lambda^2})$ for a 'steadily' driven turbulence in a periodic domain without boundary. It should be noted that in their expression (28) of $\overline{\epsilon}$, Doering & Foias (2002) used the following form for the time-independent forcing, $f = F\Phi(x/l)$ with $l = \alpha L$ where α and L are an integer and the size of the system, respectively. More recently, McComb *et al.* (2015) used the Kármán–Howarth equation with a forcing term to develop a model for C_ϵ for forced homogeneous isotropic turbulence (HIT). Using L as a scaling length scale and applying asymptotic expansions for the second- and third-order velocity structure functions into the Kármán–Howarth equation, they obtained $C_\epsilon = C_{\epsilon,\infty} + C/Re_L$, where $C_{\epsilon,\infty} = 0.468 \pm 0.006$ and $C = 18.9 \pm 1.3$ are constant with respect to Re_L and the dimensionless variable r/L. Further, they used the expression $Re_L = C_\epsilon Re_\lambda^2/15$, albeit without justification, to show that $C_\epsilon = A(1 + \sqrt{1+(B)/Re_\lambda^2})$, where A and B are

https://doi.org/10.1017/jfm.2017.110 Published online by Cambridge University Press

constant with respect to Re_λ, which is similar to the upper bound of C_ϵ of Doering & Foias (2002). In this paper, we present a derivation for an analytical expression of C_ϵ based on the Navier–Stokes equations. The approach follows the work of Lohse (1994) and McComb *et al.* (2015), in that the starting point of the analysis is the transport equation for $\overline{(\delta u)^2}$. However, we avoid using any model closure or asymptotic expansion in the analysis, although we work within the framework of SP, which is aligned with the approach taken by both Taylor (1935) and Kolmogorov (1941*b*).

The aim of the study is to assess the Reynolds number dependence of C_ϵ in decaying turbulence. Two cases of decaying turbulence are considered: HIT such as closely approximated in grid turbulence and locally homogeneous and isotropic turbulence such as on the axis of a turbulent round jet (§ 2). The analytical results are tested against the experimental data in § 3. It should be stressed that the quest for an answer to the issue regarding whether or not C_ϵ is Reynolds number dependent or has a universal value (i.e. independent of the Reynolds number and flow configurations) has an important practical implication considering that $\overline{\epsilon}$ plays a fundamental role in the theory of turbulence and is a critical controlling variable in many processes (e.g. mixing, chemical reactions, interfacial exchanges). For example, considering that $\overline{\epsilon}$ is practically impossible to measure during field experiments (e.g. atmospheric, oceanic and industrial measurements) the knowledge (i) that C_ϵ is universal and (ii) of its actual value would greatly benefit such experiments. Indeed, if C_ϵ is a universal constant, then it allows a relatively simple practical way for estimating $\overline{\epsilon}$ in any turbulent flow, at least at high Reynolds numbers. One would be required to measure both the turbulence intensity, u', and the integral length scale, L, which are relatively straightforward to measure.

2. Theoretical considerations

2.1. *Homogeneous and isotropic turbulence*

For the sake of convenience, we reproduce here the first stages of the SP analytical development of Djenidi & Antonia (2015) (hereafter denoted DA15), which we then extend to derive an expression for C_ϵ. The starting point of the analysis is the transport equation for the second-order velocity structure function, $\overline{(\delta u)^2}$ where the velocity increment is $\delta u = (u(x + r, t) - u(x, t))$, (Danaila *et al.* 1999; Antonia *et al.* 2003)

$$-\overline{(\delta u)^3} + 6\nu\frac{\partial\overline{(\delta u)^2}}{\partial r} - \frac{3}{r^4}\int_0^r s^4\frac{\partial\overline{(\delta u)^2}}{\partial t}\,\mathrm{d}s = \frac{4}{5}\overline{\epsilon}r, \tag{2.1}$$

where $\overline{\epsilon} = -(2/3)(\partial\overline{u^2}/\partial t)$ is the mean turbulent kinetic energy dissipation rate ((2.1) is also called the scale-by-scale (SBS) energy budget). Following Barenblatt & Gavrilov (1974), we assume the following SP expressions for $\overline{(\delta u)^2}$ and $\overline{(\delta u)^3}$ *viz.*

$$\overline{(\delta u)^2} = u_2^2(t)f(r^*) \tag{2.2}$$

$$\overline{(\delta u)^3} = u_3^3(t)g(r^*), \tag{2.3}$$

where $r^* = r/l(t)$; $l(t)$, $u_2(t)$ and $u_3(t)$ are the length scale and velocity scaling functions to be determined while f and g are dimensionless functions. For convenience, we hereafter drop the variable t. Their analysis introduces the skewness of the longitudinal velocity increment, $S(r)(\equiv \overline{(\delta u)^3}/\overline{(\delta u)^2}^{3/2})$, as a SP controlling parameter.

https://doi.org/10.1017/jfm.2017.110 Published online by Cambridge University Press

Using (2.2) and (2.3), one can write $S = c(t)\phi(r/l)$ where $c(t)$ and $\phi(r/l)$ are dimensionless functions of time and (r/l), respectively. DA15's SP framework allowed a critical appraisal of the specific assumptions that have been made in previous SP analyses. Specifically, SP is achieved when $cRe_l = \text{const.}$, where $Re_l = u_2 l/\nu$ is the 'scaling' Reynolds number. DA15 further show that when $c(t)$ is constant, then $Re_l = \text{const.}$, the length scale l can hence be identified not only with the Kolmogorov length scale η, but with any other characteristic length scale which is proportional to η. The implication is that SP is complete or exact i.e. the ratio between any two length scales is constant (similarly for any two velocity scales) even when Re_l is relatively small. Recent measurements in the far field of a cylinder wake (Tang *et al.* 2015*b*) show that $S(r)$ collapses onto a single distribution, confirming that $S = c(t)\phi(r/l)$ with $c(t) = \text{const.}$ (i.e. $Re_l = \text{const.}$). This is remarkable considering that the turbulence in the far wake is neither homogeneous nor isotropic, and the Taylor microscale Reynolds number is small. This suggests that the DA15 SP analysis can be extended to anisotropic turbulence and in particular that the SP constraint $cRe_l = \text{const.}$ appears to be a general requirement that needs to be satisfied in any turbulent flow if SP is to be achieved. This constraint presents two cases of SP, discussed in DA15. One, as observed in Tang *et al.* (2015*b*) (see their figure 13), in which $c(t)$ is constant and the second which allows $c(t)$ to vary. However, so far, experimental and numerical evidence show that SP is observed when Re_l is constant during decay, implying that $c(t)$ is constant too. The case of non-constant $c(t)$ under SP is yet to be observed. Accordingly, the SP analysis presented below concerns mainly SP where $c(t)$ is constant during the decay, which we know can be observed experimentally and numerically.

Following Djenidi & Antonia (2015), we substitute (2.2), (2.3) and $S(r)$ into (2.1). After some trivial manipulations, we obtain

$$6f'(r^*) - \frac{cu_2 l}{\nu}\phi(r^*)f(r^*)^{3/2} - \frac{3l^2}{\nu u_2^2}\frac{\partial u_2^2}{\partial t}\frac{\Gamma_1}{r^{*4}} + \frac{3}{\nu}l\frac{\partial l}{\partial t}\frac{\Gamma_2}{r^{*4}} = \frac{4}{5}\frac{\overline{\epsilon}}{\nu u_2^2}l^2 r^*, \tag{2.4}$$

with

$$\Gamma_1 = \int_0^{r^*} s^{*4} f(s^*)\,\mathrm{d}s^* \tag{2.5}$$

$$\Gamma_2 = \int_0^{r^*} s^{*5} f'(s^*)\,\mathrm{d}s^*, \tag{2.6}$$

where s^* is a dummy variable of integration. Equation (2.4) holds at all scales if $\Gamma_1 \sim r^{*5}$ and $\Gamma_2 \sim r^{*5}$ when $r^* \to \infty$. Since $f(r^*) \to \text{const.}$ and $f'(r^*) \to 0$ when $r^* \to \infty$, it is easy to show that these conditions are satisfied. Note also that when $r^* \to 0$, $f \sim r^{*2}$. Thus, $\Gamma_1 \sim r^{*7}$ and $\Gamma_2 \sim r^{*7}$; they approach zero more rapidly than r^{*4}.

The SP constraints are:

$$cRe_l = C_0 \tag{2.7}$$

$$\frac{l^2}{\nu u_2^2}\frac{\partial u_2^2}{\partial t} = C_1 \tag{2.8}$$

$$\frac{l}{\nu}\frac{\partial l}{\partial t} = C_2 \tag{2.9}$$

$$\frac{\overline{\epsilon} l^2}{\nu u_2^2} = C_3, \tag{2.10}$$

https://doi.org/10.1017/jfm.2017.110 Published online by Cambridge University Press

where $Re_l = u_2 l/\nu$ is a scaling Reynolds number. Evidently, the above constraints, i.e. C_i must be independent of t (since the coefficient of the first term on the left-hand side of (2.4) is a constant), apply for all separations r^* while the numerical value of the constants C_i depend on the scaling variables. Combining (2.7) and (2.10) and using the definition of Re_l yields

$$l = \left(\frac{\sqrt{C_3}C_0}{c}\right)^{1/2}\left(\frac{\nu^3}{\overline{\epsilon}}\right)^{1/4}. \tag{2.11}$$

Now, substituting (2.11) into (2.10) leads to

$$u_2 = \left(\frac{C_0}{\sqrt{C_3}c}\right)^{1/2}(\nu\overline{\epsilon})^{1/4}. \tag{2.12}$$

Recognizing that $\eta = (\nu^3/\overline{\epsilon})^{1/4}$ and $v_K = (\nu\overline{\epsilon})^{1/4}$, the Kolmogorov length and velocity scales, respectively, we can write $l = C_\eta\eta$ and $u_2 = C_{v_K}v_K$. Clearly, C_η and C_{v_K} are constant if c or equivalently Re_l is constant. So far, experimental and numerical evidence indicate that SP occurs when the scaling Reynolds number is constant. We thus will take c or Re_l to be constant under SP. Note that if c is constant, one can, without loss of generality, take $u_3 = u_2$ and (2.7) becomes $Re_l = C_0$. Expressions (2.11) and (2.12) reveal that, under SP, $\overline{\epsilon}$ and ν are the relevant natural parameters for the velocity increments.

The above derivation of the SP constraints (2.7)–(2.10) is similar to that of DA15. The rest of the analysis departs from DA15. We can now rewrite (2.4) as

$$-S(r^*) = f(r^*)^{-3/2}\frac{1}{Re_l}\left\{-6f'(r^*) + \frac{4}{5}C_3 r^* + \frac{3}{r^{*4}}(C_1\Gamma_1 - C_2\Gamma_2)\right\}. \tag{2.13}$$

$C_1 = -2C_2$ under SP (DA15), then

$$-S(r^*) = -6\frac{f(r^*)^{-3/2}f'(r^*)}{Re_l} + \frac{f(r^*)^{-3/2}}{Re_l}\left\{\frac{4}{5}C_3 r^* + \frac{3}{r^{*4}}C_1\left(\Gamma_1 + \frac{1}{2}\Gamma_2\right)\right\}. \tag{2.14}$$

First we write (2.14) as

$$-S(r^*)f(r^*)^{3/2} = -6\frac{f'(r^*)}{Re_l} + \frac{1}{Re_l}\left\{\frac{4}{5}C_3 r^* + \frac{3}{r^{*4}}C_1\left(\Gamma_1 + \frac{1}{2}\Gamma_2\right)\right\}. \tag{2.15}$$

If $l = \lambda$ and $u_2 = u'$ (i.e. λ and u' are scaling variables satisfying SP requirements) and writing $C_{3,\lambda} = (\epsilon\lambda^2/\nu u'^2) = C_\epsilon(\lambda/L)Re_\lambda$, we have the following expression for C_ϵ:

$$C_\epsilon = 15\frac{L}{\lambda}\frac{1}{Re_\lambda} = \left\{-\frac{5}{4}S(r^*)f(r^*)^{3/2} + \frac{15}{2}\frac{f'(r^*)}{Re_\lambda} - \frac{1}{Re_\lambda}\left(\frac{15}{4r^{*4}}C_1\left(\Gamma_1 + \frac{1}{2}\Gamma_2\right)\right)\right\} * \frac{r_L^*}{r^*}, \tag{2.16}$$

where $r_L^* = L/\lambda$ and $C_{3,\lambda} = 15$; L is a length scale characteristic of the large-scale motions. This expression reveals a non-trivial Re_λ dependency of C_ϵ felt at all scales of motion. Also, C_ϵ must be independent of r^*, which is easily verified. For example, when $r^* \to \infty$, we obtain these asymptotic values, $f(r^*) \simeq 2$, $f'(r^*) = 0$, $S(r^*) = 0$. Then it follows that $\Gamma_1 \simeq (2/5)r^{*5}$, $\Gamma_2 \simeq 0$ and the right-hand side of (2.16) becomes

$$C_\epsilon = 15\frac{L}{\lambda}\frac{1}{Re_\lambda} = 15\frac{Re_L}{Re_\lambda^2}, \tag{2.17}$$

https://doi.org/10.1017/jfm.2017.110 Published online by Cambridge University Press

where $r_L^* = Re_L/Re_\lambda$ and $C_1 = -10$ (for HIT under SP, i.e. constant Re_λ; see DA15). We can also recover this expression when $r^* \to 0$. Indeed, expanding $f(r^*)$ around $r^* = 0$ and using Taylor series expansion to order 4 yields

$$f(r^*) \simeq \alpha r^{*2} - \tfrac{1}{12}\beta r^{*4}, \tag{2.18}$$

where $\alpha = (l^2/u_2^2)\overline{(\partial u/\partial x)^2}$ and $\beta = (l^4/u_2^2)\overline{(\partial^2 u/\partial x^2)^2}$ are constant under SP and whose values depend on the choice of l and u_2. Since we selected $u_2 = u'$ and $l = \lambda$ then $\alpha = 1$, and $\beta = G = (u'^2\overline{(\partial^2 u/\partial x^2)^2}/\overline{(\partial u/\partial x)^2}^2)$, often called the enstrophy destruction coefficient of $\bar{\epsilon}$. Substituting (2.18) into (2.16) with $(\Gamma_1 + 1/2\Gamma_2) = (2/7)r^{*7}$ as $r^* \to 0$ yields

$$C_\epsilon = \left(-\frac{5}{4}S_{(r^*\to 0)} - \frac{5}{2}\frac{G}{Re_\lambda} + \frac{15}{14}\frac{C_1}{Re_\lambda}\right) r^{*2}\frac{L}{\lambda} + 15\frac{L}{\lambda}\frac{1}{Re_\lambda}, \tag{2.19}$$

which leads to $C_\epsilon \simeq 15(L/\lambda)/Re_\lambda$ for very small r^*. The expression inside the parentheses is of interest. Since C_ϵ must be independent of r^*

$$-S_{(r^*\to 0)} - 2\frac{G}{Re_\lambda} + \frac{6}{7}\frac{C_1}{Re_\lambda} = 0. \tag{2.20}$$

This expression, which is in fact the transport equation for $\bar{\epsilon}$ first written and tested by Batchelor & Townsend (1947) and analysed in detail by Djenidi & Antonia (2014) using direct numerical simulation based on the lattice Boltzmann method (Succi 2001), was recently extensively used to determine the behaviours of $S_{(r^*\to 0)}$ and G when $Re_\lambda \to \infty$ in several turbulent flows (Lee *et al.* 2013; Thiesset, Antonia & Djenidi 2014; Antonia *et al.* 2015; Tang *et al.* 2015*a*,*b*,*c*) in the context of assessing whether the small-scale statistics are consistent with the original similarity hypothesis (Kolmogorov 1941*a*) or the modified one (Kolmogorov 1962), i.e. whether $S_{(r^*\to 0)} \to$ const. or $S_{(r^*\to 0)} \sim Re_\lambda^\alpha$; $S_{(r^*\to 0)}$ is the velocity derivative skewness. If one accepts that C_ϵ approaches a constant as Re_λ increases, then one must accept that (2.20) holds. Thus, since C_1 is constant ($\equiv -10$), equation (2.20) reduces to $S_{(r^*\to 0)} + 2G/Re_\lambda \to 0$ as Re_λ increases.

We can write (2.16) in the generic form

$$C_\epsilon = \left\{A(r^*) + \frac{B(r^*)}{Re_\lambda}\right\}\frac{L}{\lambda}, \tag{2.21}$$

where $A(r^*)$ and $B(r^*)$ are functions of r^*, possibly of the Reynolds number too, and

$$A(r^*) + \frac{B(r^*)}{Re_\lambda} = \frac{15}{Re_\lambda}. \tag{2.22}$$

We can easily relate C_ϵ to the SP constants C_0 and C_3. If we rewrite (2.7) as

$$l = \frac{C_0\nu}{cu_2} \tag{2.23}$$

and substitute it into (2.10), we obtain

$$\frac{\bar{\epsilon}l}{u_2^3} = \frac{C_3 c}{C_0}. \tag{2.24}$$

https://doi.org/10.1017/jfm.2017.110 Published online by Cambridge University Press

If $l = L$ (i.e. L is assumed to be a scaling length satisfying the SP requirement) and $u_2 = u'$, then we have

$$\frac{\overline{\epsilon} L}{u'^3} = C_\epsilon = \frac{C_{3,L} c}{C_{0,L}} = \frac{C_{3,L}}{Re_L}, \tag{2.25}$$

where $Re_L = u'L/\nu$. Note that $C_{3,L} \neq 15$. This is readily shown as follows. In the context of SP, if both λ and L are scaling lengths then (2.10) holds for both these quantities and we have

$$C_{3,L} = \frac{L^2}{\lambda^2} 15, \tag{2.26}$$

where we used $u_2 = u'$. This leads to

$$C_\epsilon = 15 \frac{L^2}{\lambda^2} \frac{1}{Re_L} = 15 \frac{Re_L}{Re_\lambda^2}. \tag{2.27}$$

2.2. *Locally homogeneous and isotropic turbulence*

The analysis carried out above for HIT can be experimentally tested only approximately in grid turbulence, which remains, as far as we are aware, the closest approximation to HIT in the laboratory. Another flow that is amenable to a SP analysis and where HIT can be locally observed is the far field of a turbulent round jet. Burattini, Lavoie & Antonia (2005*b*) showed that the SBS energy budget on the axis of the jet is given the following generic form:

$$-\overline{(\delta u)^3} + 6\nu \frac{\partial \overline{(\delta u)^2}}{\partial r} + I_u = \frac{4}{5} \overline{\epsilon} r, \tag{2.28}$$

where I_u represents the contribution of the large-scale motions. The term I_u is

$$I_u(r) = -\frac{U}{r^4} \int_0^r s^2 \frac{\partial \overline{(\delta u)^2}}{\partial x} \, \mathrm{d}s - 6 \frac{\partial U}{\partial x} \frac{1}{r^4} \int_0^r s^4 (\overline{(\delta u)^2} - \overline{(\delta v)^2}) \, \mathrm{d}s \tag{2.29}$$

and represents the contributions from the advection (first term) and production (second term) mechanisms, respectively. Darisse, Lemay & Benaissa (2015) showed that the energy contribution from the pressure diffusion, turbulent diffusion and molecular diffusion are negligible in the turbulent kinetic energy budget on the axis of the round jet, which allows us to neglect them in $I_u(r)$. Seeking SP solutions of similar forms as (2.2) and (2.3) and after following the same trivial manipulations as above we obtain

$$C_\epsilon = -\frac{5}{4} S(r^*_{L_u}) f_u(r^*_{L_u})^{3/2} + \frac{15}{2} \frac{f'_u(r^*_{L_u})}{Re_\lambda} \frac{r^*_{L_u}}{r^*} - \frac{1}{Re_\lambda} \frac{r^*_{L_u}}{r^*} \left\{ \frac{15}{4 r^{*4}_{L_u}} (C_2 \Gamma_1 - C_3 \Gamma_2 + 2 C_4 \Gamma_3) \right\}, \tag{2.30}$$

where Γ_1 and Γ_2 are similar to (2.5) and (2.6), respectively, and

$$\Gamma_3 = \int_0^{r^*} s^{*2} (f_u(s^*) - f_v(s^*)) \, \mathrm{d}s^*. \tag{2.31}$$

In the Appendix we reproduce, for the sake of convenience, the first stages of the analytical development of Djenidi *et al.* (2016) for the transport equation of $\overline{(\delta q)^2} = \overline{(\delta u)^2} + \overline{(\delta v)^2} + \overline{(\delta w)^2}$ and then develop a similar expression to (2.30), albeit with different numerical coefficients.

The objective of the next section is to test the analysis against experimental data in grid turbulence and on the axis of a turbulent round jet.

https://doi.org/10.1017/jfm.2017.110 Published online by Cambridge University Press

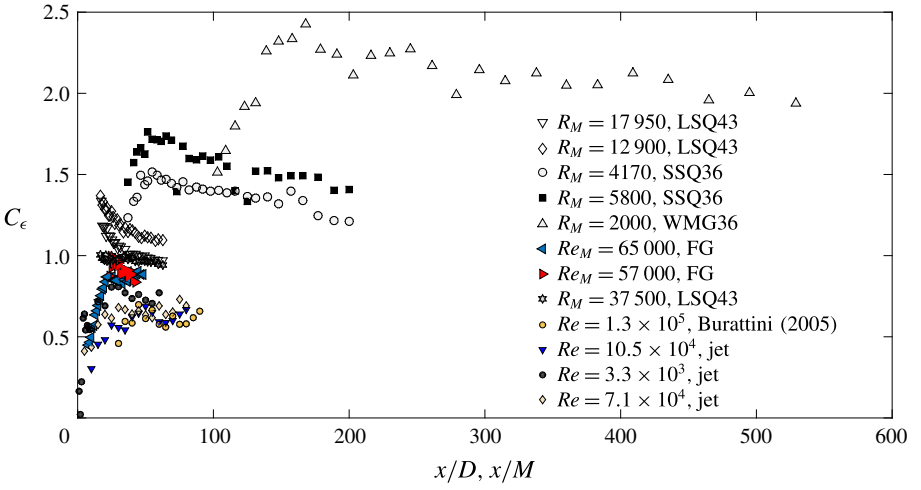

FIGURE 1. (Colour online) Streamwise variation of C_ϵ in grid turbulence and on the axis of a round jet. LSQ43: perforated plate with large square holes with solidity 43 %; SSQ36: perforated plate with small square holes with a solidity 36 %; WMG36: woven mesh grid with a solidity 36 %; FG: fractal grid; for FG, M corresponds to the mesh size of the background grid supporting the fractal elements.

3. Discussion and experimental results

The theoretical analysis developed above indicates that the constancy of C_ϵ in a decaying turbulence for a given Reynolds number is a consequence of the turbulence decaying under the SP requirement. To assess these theoretical results, we report measurements of C_ϵ in decaying grid turbulence and on the axis of a turbulent round jet in figure 1. Whilst grid turbulence does not satisfy SP (Djenidi *et al.* 2015), the far-field flow along the jet axis complies well with SP (Djenidi *et al.* 2016). The measurements in grid turbulence were made using three different grids; two were constructed from perforated plates, but with different (square) hole sizes (denoted LSQ43 and SSQ36, 46 and 36 % solidity), and one is a woven mesh (WMG36, 36 % solidity). Details of the grid turbulence experiments can be found in Djenidi *et al.* (2015), while details of the round jet measurements can be found in Djenidi *et al.* (2016). Figure 1 reports also the measurements of Hearst & Lavoie (2014) obtained in fractal grid (FG) turbulence and the results of Burattini, Antonia & Danaila (2005*a*) in the turbulent round jet. All values of C_ϵ are calculated using L defined as

$$L_u = \frac{1}{\overline{u^2}} \int_0^{r_o} \overline{u(x)u(x+r)}\, \mathrm{d}r, \tag{3.1}$$

where r_o is the first zero crossing of the auto-correlation of the longitudinal velocity. The trend in the variation of C_ϵ along x in grid turbulence is clear: C_ϵ decreases with increasing x. This is consistent with the measurements of Krogstad & Davidson (2011) in decaying turbulence downstream of multiscale grids. For the SSQ and WMG data, C_ϵ first increases before decreasing. The increase reflects the non-homogeneity of the turbulence which is still in a development stage immediately downstream of the grid. This region expands as Re_M decreases, as the comparison between the SSQ and LSQ data illustrates. This region is further extended behind a FG as Hearst &

https://doi.org/10.1017/jfm.2017.110 Published online by Cambridge University Press

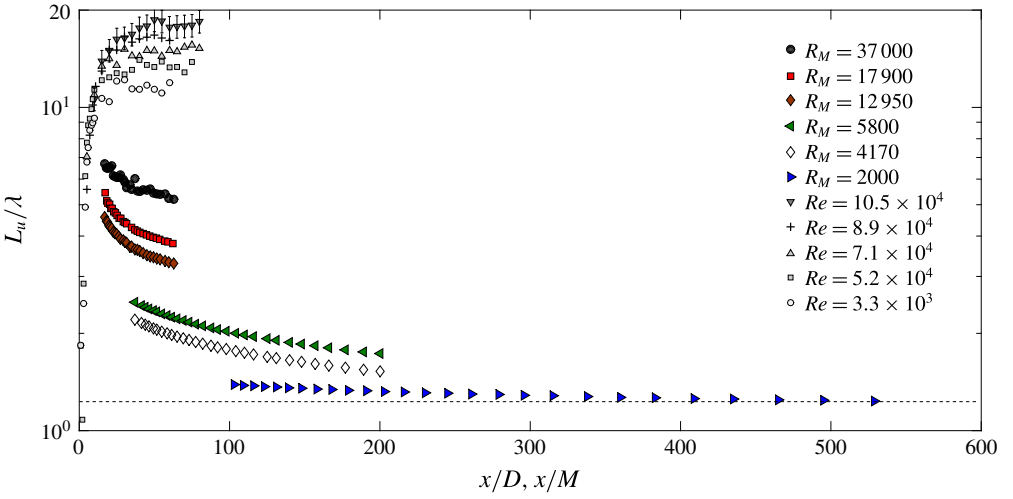

FIGURE 2. (Colour online) Streamwise variation of L_u/λ in grid turbulence and along the axis of a turbulent round jet. The dashed line is used only as a visual guide to make it clearer that the data for $R_M = 2000$ actually decrease as x increases.

Lavoie (2014) showed in their comparative study between a classical grid and a FG. After an initial increase behind the FG, C_ϵ appears to decrease. However, a much longer distance is required to assess the definitive trend for this type of grid turbulence. The data for the round jet indicate that C_ϵ remains practically constant along the axis for a given Reynolds number, after an initial increase. The variation of C_ϵ with x/M in grid turbulence is consistent with a lack of SP at all scales of motion. Djenidi *et al.* (2015) showed that decaying grid turbulence obtained in the laboratory is not in SP. Their experimental results confirm the results of the eddy-damped quasi-normal Markovian (EDQNM) simulation of decaying HIT by Meldi & Sagaut (2013) and the analysis of Djenidi & Antonia (2015) for decaying HIT. The latter derived an analytical expression relating the power-law decay exponent n and Re_λ, which shows that SP at all scales of motion can only be achieved if $Re_\lambda \simeq \infty$ or finite Re_λ provided Re_λ is constant, which would lead to $n = -1$. So far, experimental and numerical evidence point to a decrease in Re_λ in decaying HIT. By contrast, the constancy of C_ϵ on the jet axis reflects the validity of SP at all scales of motion (e.g. Burattini *et al.* 2005*a*; Djenidi *et al.* 2016). Djenidi *et al.* (2016) showed analytically that the requirement for SP on the axis of a turbulent round jet is similar to that for decaying HIT (i.e. constancy of Re_λ). Their measurements along the jet axis showed not only that Re_λ is constant, but both the one-point and two-point turbulence statistics evolve in a manner which complies with SP, in the far field. Accordingly, for a given initial condition, (i.e. a given global Reynolds number such as Re_M in grid turbulence or Re_D for a jet), one should expect that C_ϵ varies with x in decaying grid turbulence, and to remain constant along the axis in the far field of a turbulent round jet.

Likewise, SP at all scales of motion also implies that $r_L^* = L/\lambda$ must be a constant as the turbulence decays at any one Reynolds number. We show in figure 2 the variation of $L_u/\lambda (= r_{L_u}^*)$ with x for the data reported in figure 1; a log scale is used for the ordinate to highlight more effectively any streamwise variation at small $r_{L_u}^*$. In grid turbulence, $r_{L_u}^* \simeq 3.3$–7 for LSQ43, $r_{L_u}^* \simeq 1.5$–2.5 for SSQ43, $r_{L_u}^* \simeq 1.1$–1.25 for WMG36 (the measurement uncertainties are 6 %, 7.3 % and 9.65 % for LSW, SSQ

https://doi.org/10.1017/jfm.2017.110 Published online by Cambridge University Press

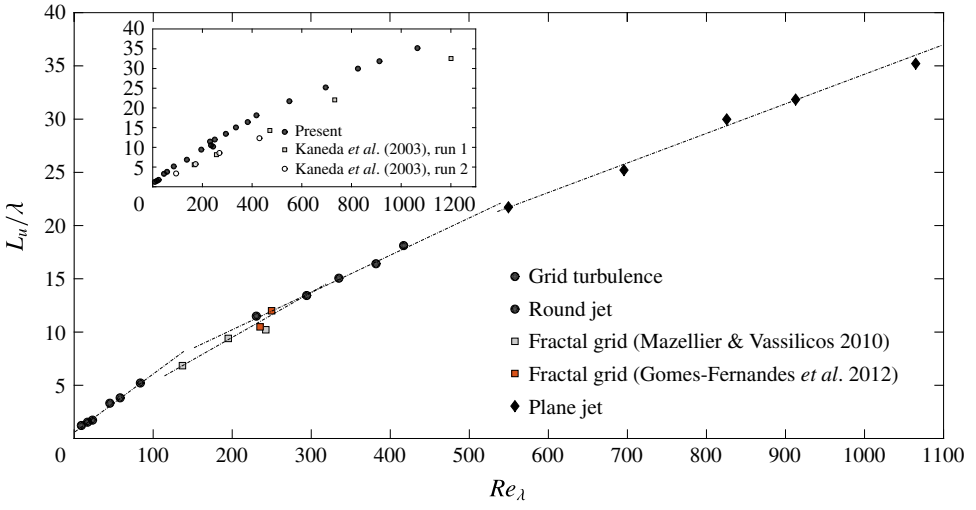

FIGURE 3. (Colour online) Dependence of L_u/λ on Re_λ in grid turbulence and along the axis of a turbulent round jet and a plane jet. The dashed line is a linear fit used only as reference for the behaviour $L_u/\lambda \sim Re_\lambda$. The data for Gomes-Fernandes, Ganapathisubramani & Vassilicos (2012) are for two fractal grids defined as SFG8 and SFG17 with the same solidity. Inset: comparison between the distributions of the main plot (black circles) with the distribution from the forced HIT of Kaneda *et al.* (2003).

and WWG, respectively). For the FG data (not shown here), $r^*_{L_u} \simeq 6$–7.3 and decreases with x; Re_λ also decreases (see figure 10 of Hearst & Lavoie (2014)). The variation of $r^*_{L_u}$ with x is consistent with a lack of SP. On the jet axis, the ratio $r^*_{L_u}$ increases initially at a steep rate. It then approaches a plateau, notwithstanding the jitter in the data at high x/D, associated with the difficulty in determining the first zero crossing of the velocity auto-correlation function; the distance x/D for the $r^*_{L_u}$ distributions to approach a plateau increases with the Reynolds number. This is consistent with the observation that the onset of the SP solutions moves downstream as Re_D increases. For example, Djenidi *et al.* (2016) showed that SP starts at $x/D \simeq 15$ and 40 when $Re_D = 3.4 \times 10^4$ and 13×10^4, respectively. It should be noted that these far-field measurements in a turbulent jet are difficult because the turbulence intensity becomes (i) low and (ii) susceptible to the environment (the measurement uncertainty in L_u varies from 8 % for $Re_D = 33\,000$ to 15 % for $Re_D = 105\,000$). This explains in part the jitter in the data and why far-field data are rather scant in a turbulent jet.

For a given flow configuration, the streamwise behaviour of $r^*_{L_u}$ with downstream distance is independent of the 'inlet' Reynolds number, Re_D for the jet and Re_M for grid turbulence: $r^*_{L_u}$ becomes constant after an increase in the former case, while it decreases continuously in the latter. However, for both flows, $r^*_{L_u}$ increases with the 'inlet' Reynolds number or equivalently with Re_λ. This is well illustrated in figure 3, which shows the variation of $r^*_{L_u}$ with Re_λ. The value of $r^*_{L_u}$ for each grid turbulence is taken at the last x/M position, while for the round jet we used the value of $r^*_{L_u}$ averaged over the region over which it is practically constant. Sreenivasan (1984) showed that $L_u/\lambda \simeq (\pi/2)^{1/2}$ for grid turbulence at very low Reynolds numbers where the energy transfer is very weak such as in the final period of decay. The present results suggest that the final period of decay has not yet been reached, even though the smallest Re_λ is approximately 9 in the woven mesh grid turbulence. Note however

https://doi.org/10.1017/jfm.2017.110 Published online by Cambridge University Press

that Djenidi *et al.* (2014) showed that the Kolmogorov scaling breaks down when Re_λ drops below approximately 20, underlining the persistence of the Reynolds number dependence of L_u/λ. We have also added data for a plane jet (Pearson & Antonia 2001; Zhou, Pearson & Antonia 2001) and the fractal grid turbulence of Mazellier & Vassilicos (2010) (see also figure 3 in Vassilicos (2015)) and Gomes-Fernandes *et al.* (2012) (for both fractal grids only the last x station was used, but similar results are observed upstream of that position). It is evident that $r^*_{L_u}$ increases with increasing Re_λ, regardless of the flow configuration. Further, the data seem to collapse remarkably and unexpectedly well onto a single line, as suggested in the inset of figure 3 where the data are redrawn but without differentiating between the sets of data. For comparison, we have reported $r^*_{L_u}$ for the high Reynolds number direct numerical simulation (DNS) of a three-dimensional periodic forced turbulence or forced HIT (Kaneda *et al.* 2003). It seems that the distribution of $r^*_{L_u}$ for all decaying turbulence (black circles) tends to become parallel to the $r^*_{L_u}$ distribution of forced turbulence as Re_λ increases. Note the latter is relatively well represented by $L_u/\lambda \sim Re_\lambda$ for the whole range of Re_λ used, although there is a deviation from that behaviour for the largest Reynolds number. At this stage, it is unfortunately not possible to determine whether or not the curve formed by the black circles will eventually remain parallel to the data for forced HIT and thus behave like $L_u/\lambda \sim Re_\lambda$. If, from a purely practical point of view, one considers the flow configurations separately, one may argue that, in a first approximation, $L_u/\lambda \sim Re_\lambda$ with the constant of proportionality changing between the flows (this is represented by the dashed-dotted lines). It is interesting to note that it is perhaps not a coincidence that the value of the constant of proportionality corresponds to different ranges of Re_λ, and that it decreases as Re_λ increases. Applying a simple linear curve fit to each set of data (grid turbulence, round jet and plane jet) of figure 3 we then obtain

$$r^*_{L_u} \simeq a^\dagger + b^\dagger Re_\lambda, \tag{3.2}$$

where the pair of coefficients $(a^\dagger, b^\dagger)$ is (0.6, 0.0533), (1.23, 0.042), (3, 0.0357) and (6.015, 0.0281) for the grid turbulence, the fractal grid turbulence and the axes of the round and plane jets, respectively (the symbol † in (3.2) and in (3.3), below, is a reminder that the empirical constants, which, by the empirical nature of their derivation, may be Reynolds number dependent and flow dependent). Using (2.17) with (3.2) yields the following empirical relation for C_ϵ

$$C_\epsilon \simeq \frac{c^\dagger}{Re_\lambda} + d^\dagger, \tag{3.3}$$

where $(c^\dagger, d^\dagger)$ is (9, 0.7995), (18.45, 0.623), (45, 0.5355) and (90.4, 0.421) for standard grid turbulence, fractal grid turbulence, the axis of the round jet and the centreline of the plane jet, respectively. It seems that (3.3) would provide the asymptotic value $C_{\epsilon,\infty} = d^\dagger$ when $Re_\lambda \to \infty$, which would appear to depend on the flow configuration; $C_{\epsilon,\infty} \simeq 0.8$, 0.62, 0.54 and 0.42 for standard grid turbulence, fractal grid turbulence, round jet axis and plane jet centreline, respectively. These results suggest that $C_{\epsilon,\infty}$ is controlled by the rate of growth of $r^*_{L_u}$; the larger the growth, the larger $C_{\epsilon,\infty}$. This rate of growth decreases with increasing Re_λ. However, it is clear that the empirical constants obtained above are only valid for the corresponding flow configuration considered and the range of Re_λ over which the curve fit was applied, which leads to an important issue requiring further investigation and which relates to the asymptotic behaviour of $r^*_{L_u}$ with increasing Re_λ in different turbulent flows.

https://doi.org/10.1017/jfm.2017.110 Published online by Cambridge University Press

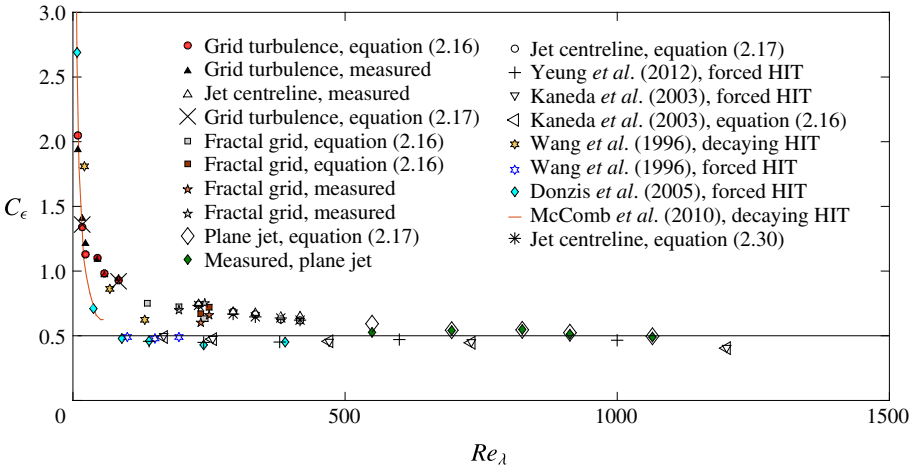

FIGURE 4. (Colour online) Dependence of C_ϵ on Re_λ in several turbulent flows.

Determining whether this behaviour is universal (i.e. the same for all turbulent flows) or not requires measurements in a various turbulent flows at very high Reynolds numbers. As stated above, if the trend shown in the inset of figure 3 is confirmed, that is $L_u/\lambda = \alpha Re_\lambda$ (α is a constant and the same for all turbulent flows) at very large Reynolds numbers, then $C_{\epsilon,\infty}$ would reach an asymptotic (universal) limit, yet to be properly determined. When Re_λ approaches infinitely large values, the turbulence reaches its isotropic steady state regardless of the turbulent flow configuration (at least away of any solid boundaries). If one accepts that such turbulence is adequately represented by forced HIT at a finite but large Reynolds number, then C_ϵ for such turbulence is equal to $C_{\epsilon,\infty}$. Thus, the possibility that $C_{\epsilon,\infty}$ is a universal constant should not be excluded.

The derivation of the empirical expression (3.3) is based on the relation (2.17) valid for isotropic or locally isotropic turbulence. Thus, a convenient and simple way to test isotropy or local isotropy is to compare the measured C_ϵ with the calculated one using (2.17). However, this requires the true dissipation $\overline{\epsilon}_t$, which necessitates the measurement of 12 terms. So far, only in grid turbulence can $\overline{\epsilon}_t$ be estimated reliably from the turbulence kinetic energy budget in HIT ($\overline{\epsilon}_t = -(U_o)(\mathrm{d}k/\mathrm{d}x)$, U_o is the local velocity). Of course, $\overline{\epsilon}_t$ is easily calculated with DNS data. Often in measurements, $\overline{\epsilon}_t$ is approximated by its (local) isotropic surrogate $\overline{\epsilon}_{iso}$. We reported in figure 4 the measured C_ϵ and the calculated one using (2.17) for the same flows as reported in figure 3; we also added the DNS data for forced HIT (Wang *et al.* 1996; Donzis, Sreenivasan & Yeung 2005; Yeung, Donzis & Sreenivasan 2012). For grid turbulence, we used $\overline{\epsilon}_t$ while for the two jets we used $\overline{\epsilon}_{iso}$. For the jet flows, it was found that $\overline{\epsilon}_{iso}$ is a reasonable surrogate for $\overline{\epsilon}$ (Darisse *et al.* (2015); Djenidi *et al.* (2016) for the round jet, and Antonia, Anselmet & Chambers (1986) for the plane jet), justifying the use of $\overline{\epsilon}_{iso}$; in any case, the comparison between $C_{\overline{\epsilon}_{iso}}$ and (2.17) constitutes a check for self-consistency. Also reported in the figure, are the values calculated using the second equality of (2.16) for grid turbulence where we evaluated all the terms on the right-hand side at $r = L_u$; in the case of the round jet, we used (2.30) in which we ignored the term Γ_3 because we did not have the data for $f_v(r)$. Of course, this is strictly not correct, and the values of C_ϵ obtained with (2.30) will be only an approximation. Note though that one should expect Γ_3 to be smaller than Γ_1 since

https://doi.org/10.1017/jfm.2017.110 Published online by Cambridge University Press

$(f_u(r) - f_v(r))$ is smaller than $f_u(r)$. There is a general good agreement between the measured C_ϵ and that calculated using either (2.17) or (2.16) and (2.30) for each turbulent flow. The agreement between the measurements and (2.17) for the grid turbulence indicates that local isotropy is well approximated. For forced HIT where all turbulence statistics are time independent, the agreement is perfect. Notice also the good agreement between the forced HIT data obtained in various DNS studies. For the round jet, the measurements too agree well with (2.17). This is not surprising since the constraint (2.10), which leads to $C_\epsilon = 15(L/\lambda)(1/Re_\lambda)$, applies equally to equation (2.28) and we used ϵ_{iso} as a surrogate to ϵ. The agreement with (2.30) is not as good (notice the systematic downward shift), possibly due to the neglect of Γ_3. Whilst the agreement between (2.30) and the measurements is expected because the turbulence decays in conformity with SP on the jet axis, the agreement observed for grid turbulence between the measurements and (2.16) may be less evident, since SP is strictly not satisfied, as can be seen in figure 1. The most possible explanation for this rather unexpected observation relates to the fact that the large-scale inhomogeneity in grid turbulence is weak, as reflected in the weak decrease of Re_λ with the distance x/M; the lower the initial Reynolds number, the smaller the rate of decrease. If this inhomogeneity is small enough for allowing Re_λ to be considered approximately constant over the distance x/M covered by the measurements, then one can expect to observe an approximately constant C_ϵ over that distance. Interestingly, the observation that the measurements satisfy both equalities of (2.16) suggests that local isotropy and SP are verified by the small scales even though globally both SP and isotropy are not strictly satisfied. While direct comparisons between DNS and experiments of HIT are not possible, one can still compare decaying grid turbulence, a close surrogate for decaying HIT, to DNS data for decaying HIT. To carry out such a comparison, we report in figure 4 the data of Wang *et al.* (1996) for decaying HIT. The DNS data follow the measurement trend adequately, thus lending confidence in the measurements.

The behaviour of C_ϵ depicted in figure 4 is similar to that reported by McComb (2014) (see also Kaneda *et al.* 2003; Burattini *et al.* 2005*b*) for DNS data of decaying and forced HIT. It is worthwhile commenting on this similarity considering that none of the turbulent flows investigated here, with the exception of grid turbulence, are considered HIT nor are they in 'steady state' (they decay spatially). Although it should be pointed out that while grid turbulence and the jets decay in the direction of the mean flow, there is still some 'forcing' associated with the large-scale non-homogeneity, as seen in (2.1) and (A 1). Kaneda *et al.* (2003) reported that C_ϵ can be grouped in two groups when $Re_\lambda \leqslant 250$, which was also noted by Sreenivasan (1998): decaying HIT and forced HIT. However, the two groups merge as Re_λ increases beyond 250 and C_ϵ becomes independent of Re_λ. Figure 4 also shows that while the data for forced HIT can be clearly distinguished from those for grid turbulence and jets when $Re_\lambda \leqslant 500$, they tend to merge at higher Re_λ where C_ϵ appears to become independent of Re_λ. These observations lead naturally to the issue of the universality of C_ϵ (i.e. the Re_λ independence of C_ϵ for any flow). Unfortunately, it is not possible to address this question at present but, as figure 4 shows, it is essential that any assessment of this universality to be carried out at very large Reynolds numbers.

Finally, it is worth commenting on the following seemingly paradox: the present analysis indicates that, under SP, C_ϵ (or any SP constant) remains constant during decay and yet its value can vary with the Reynolds number as seen in figure 1. This paradox may be cleared by considering the two forms of similarity hypothesis

https://doi.org/10.1017/jfm.2017.110 Published online by Cambridge University Press

introduced by Townsend (1956). The first similarity hypothesis asserts that at sufficiently high Reynolds numbers non-dimensional mean-value functions are independent of the Reynolds number; this is often called Reynolds number similarity. The second similarity hypothesis is that of self-preservation at any one Reynolds number, where the flow structure at all values of t (or x in the case of spatially evolving turbulent flows) is similar. Figure 1 illustrates the second similarity hypothesis for the round jet centreline: SP is satisfied at different Reynolds numbers, as illustrated by the constancy of both Re_λ and C_ϵ along x. On the other hand, figure 4 illustrates the Reynolds number similarity, where C_ϵ becomes independent of as Re_λ becomes large. Townsend stated that 'if, as must be assumed, Reynolds number similarity of self-preserving flows exits, the form of the self-preserving functions are universal for any one type of flow'. The question that remains to be answered is: are all turbulent flows at an infinitely large Reynolds number of one type only? The fate of the universality of C_ϵ may well rest on the answer to this question.

4. Conclusions

It is shown that, for decaying HIT and decaying local HIT, C_ϵ can be recovered from the Navier–Stokes equations when self-preservation is assumed, thus avoiding the use of dimensional analysis for its derivation. It is further shown that C_ϵ is intimately related to SP requirements, which fits well with Taylor's initial introduction of C_ϵ. When the turbulence decays/evolves in accordance with SP requirements, C_ϵ remains constant for a given flow condition. Measurements in grid turbulence, which do not satisfy SP, and a turbulent round jet, which comply with SP in the far field, confirm these analytical results. The measurements show that after an initial increase associated with the development of turbulence, C_ϵ decreases with increasing x in grid turbulence and is constant along the axis in the far field of a round jet. However, the measurements also show that C_ϵ decreases when the Reynolds number (e.g. Re_λ) increases in grid turbulence, a round jet and a plane jet. The rate at which C_ϵ decreases continues to diminish as Re_λ increases. This trend, in agreement with earlier studies (e.g. Sreenivasan 1984; Pearson, Krogstad & van de Water 2002), suggests that one cannot exclude the possibility that C_ϵ decreases towards a universal constant, which would be equal to the magnitude of C_ϵ in forced HIT, i.e. approximately 0.5.

A final word may be worthwhile on the SP solutions of the present analysis. Both the theory and experiments show that Re_λ is constant under SP. However, the theory also shows that SP under which Re_λ varies can exist. Whether or not this form of SP leads to a constant or non-constant C_ϵ during decay cannot be answered by the present theory and is yet to be observed experimentally (or numerically), but which may well exist. This situation is reminiscent of the SP solutions of Sedov (see Batchelor 1948) who showed two possible cases of SP for HIT; one with constant Re_λ during decay and the other with Re_λ increasing with time toward an asymptotic value.

Acknowledgement

The financial support of the Australian Research Council is acknowledged.

Appendix. SP analysis of locally homogeneous and isotropic turbulence based on $\overline{(\delta q)^2}$

In § 2.2 we developed an expression of C_ϵ based on the transport equation for $\overline{(\delta u)^2}$. To make the analysis somewhat more general, here, we develop an expression of C_ϵ

https://doi.org/10.1017/jfm.2017.110 Published online by Cambridge University Press

based on the transport equation for $\overline{(\delta q)^2} = \overline{(\delta u)^2} + \overline{(\delta v)^2} + \overline{(\delta w)^2}$ whose generic form is (Burattini *et al.* 2005*a*; Djenidi *et al.* 2016):

$$-\overline{(\delta u)(\delta q)^2} + 2\nu\frac{\partial\overline{(\delta q)^2}}{\partial r} + I_q = \frac{4}{3}\overline{\epsilon}r, \tag{A 1}$$

where I_q represents the contribution of the large-scale motions which varies from flow to flow. Let us for example focus on the centreline of a turbulent round jet. The term I_q is of the form

$$I_q(r) = -\frac{U}{r^2}\int_0^r s^2\frac{\partial\overline{(\delta q)^2}}{\partial x}\,\mathrm{d}s - 2\frac{\partial U}{\partial x}\frac{1}{r^2}\int_0^r s^2(\overline{(\delta u)^2} - \overline{(\delta v)^2})\,\mathrm{d}s, \tag{A 2}$$

which represents the contributions from the advection and production mechanisms, respectively. We now follow Djenidi *et al.* (2016) and seek SP requirements for (A 1) by assuming the following SP expressions

$$\overline{(\delta q)^2} = q_*^2(x)f_q(r^*), \quad \overline{(\delta u)^2} = u_*^2(x)h_u(r^*), \tag{A 3a,b}$$

$$\overline{(\delta v)^2} = v_*^2(x)h_v(r^*), \quad \overline{(\delta w)^2} = w_*^2(x)h_w(r^*), \quad \overline{(\delta u)(\delta q)^2} = (uq)_*(x)g(r^*), \tag{A 4a–c}$$

with $r^* = r/l_q$, and l_q, q_*, u_*, v_*, w_* and $(uq)_*^{1/3}$ the length and velocity scaling functions to be determined; f_q, g, h_u, h_v and h_w are dimensionless functions. Note that $\overline{(\delta v)^2} = \overline{(\delta w)^2}$ on the axis of the jet. Let us introduce the mixed skewness increment, $S_q(r)(\equiv \overline{(\delta u)(\delta q)^2}/[\overline{(\delta u)^2}^{1/2}\overline{(\delta q)^2}])$, as a SP controlling parameter; this helps for expressing $\overline{(\delta u)(\delta q)^2}$ in terms of $\overline{(\delta q)^2}$. If SP is satisfied, then S_q has also the SP expression $S_q(r) = c_q\phi_q(r^*)$ (where c_q is in general a function of x and $\phi_q(r^*)$ a function of r^*), and we can write $(uq)_* = c_q u_* q_*^2$. Note also that since we can express f_q as

$$f_q = \frac{u_*^2}{q_*^2}h_u + \frac{v_*^2}{q_*^2}h_v + \frac{w_*^2}{q_*^2}h_w, \tag{A 5}$$

and it is independent of x, we must have $q_*^2 \sim u_*^2 \sim v_*^2 \sim w_*^2$ if SP holds. Thus, we can take $u_* = v_* = w_*$ without loss of generality. Substituting (A 3), (A 4) and the definition of $S_q(r)$ in (A 1) leads to

$$-c_q\frac{u_* l_q}{\nu}G(r^*) + 2f_q'(r^*) - \frac{Ul_q^2}{\nu u_*^2}\frac{\partial u_*^2}{\partial x}\frac{\Gamma_1}{r^{*2}} + \frac{Ul_q}{\nu}\frac{\partial l_q}{\partial x}\frac{\Gamma_2}{r^{*2}} - 2\frac{l_q^2}{\nu}\frac{\partial U}{\partial x}\frac{\Gamma_3}{r^{*2}} = \frac{4}{3}\frac{\overline{\epsilon}l_q^2}{\nu u_*^2}r^*, \tag{A 6}$$

with

$$G(r^*) = f_q(r^*)h_u^{1/2}(r^*)\phi_q(r^*) \tag{A 7}$$

$$\Gamma_1 = \int_0^{r^*} s^{*2}f_q(s^*)\,\mathrm{d}s^*, \quad \Gamma_2 = \int_0^{r^*} s^{*3}f_q'(s^*)\,\mathrm{d}s^*, \quad \Gamma_3 = \int_0^{r^*} s^{*2}(h_u(s^*) - h_v(s^*))\,\mathrm{d}s^*, \tag{A 8a–c}$$

where s^* is a dummy variable of integration. SP implies that all coefficients

$$c_q R_{l_q} = C_1 \tag{A 9}$$

https://doi.org/10.1017/jfm.2017.110 Published online by Cambridge University Press

$$\frac{Ul_q^2}{\nu u_*^2}\frac{\partial u_*^2}{\partial x} = C_2 \tag{A 10}$$

$$\frac{Ul_q}{\nu}\frac{\partial l_q}{\partial x} = C_3 \tag{A 11}$$

$$\frac{l_q^2}{\nu}\frac{\partial U}{\partial x} = C_4 \tag{A 12}$$

$$\frac{\overline{\epsilon} l_q^2}{\nu u_*^2} = C_5, \tag{A 13}$$

where $R_{l_q} = u_* l_q/\nu$ is a scaling Reynolds number, are independent of x, since the coefficient of the second term in (A 6) is a constant. We can now write

$$-S(r^*) \simeq f_q(r^*)^{-1} h_u(r^*)^{-1/2} \frac{1}{Re_{l_q}} \left\{ -2f_q'(r^*) + \frac{4}{3}C_5 r^* + \frac{1}{r^{*2}}(C_2\Gamma_1 - C_3\Gamma_2 + 2C_4\Gamma_3) \right\}. \tag{A 14}$$

After trivial manipulations we obtain:

$$\begin{aligned} C_\epsilon \;=\; & -\frac{3}{4}S(r^*_{L_q}) f_q(r^*_{L_q}) h_u(r^*_{L_q})^{1/2} \frac{r^*_{L_q}}{r^*} + \frac{3}{2}\frac{f_q'(r^*_{L_q})}{Re_{\lambda_q}}\frac{r^*_{L_q}}{r^*} \\ & - \frac{1}{Re_{\lambda_q}}\frac{r^*_{L_q}}{r^*}\left\{ \frac{3}{4r^{*2}_{L_q}}(C_2\Gamma_1 - C_3\Gamma_2 + 2C_4\Gamma_3) \right\}, \end{aligned} \tag{A 15}$$

where we used $l_q = \lambda_q$ $(q = 2k)$ and $u_* = q^{1/2}$ $(q = 2k)$. We can now apply similar arguments as in HIT to find an expression for C_ϵ when r^* is large enough so that $f_q = h_u = h_v \simeq 2$ and $S(r^*) = 0$. This leads to

$$C_\epsilon \simeq -\frac{1}{2}C_2\frac{Re_{L_q}}{Re^2_{\lambda_q}} = \frac{1}{2}C_2\frac{1}{Re_{\lambda_q}}\frac{L_q}{\lambda_q}, \tag{A 16}$$

which is equivalent to the isotropic form (2.17).

REFERENCES

ANTONIA, R. A., ANSELMET, F. & CHAMBERS, A. J. 1986 Assessment of local isotropy using measurements in a turbulent plane jet. *J. Fluid Mech.* **163**, 365–391.

ANTONIA, R. A., SATYAPRAKASH, B. R. & HUSSAIN, A. K. M. F. 1980 Measurements of dissipation rate and some other characteristics of turbulent plane and circular jets. *Phys. Fluids* **23**, 695–700.

ANTONIA, R. A., SMALLEY, R. J., ZHOU, T., ANSELMET, F. & DANAILA, L. 2003 Similarity of energy structure functions in decaying homogeneous isotropic turbulence. *J. Fluid Mech.* **487**, 245–269.

ANTONIA, R. A., TANG, S. L., DJENIDI, L. & DANAILA, L. 2015 Boundedness of the velocity derivative skewness in various turbulent flows. *J. Fluid Mech.* **781**, 727–744.

BARENBLATT, G. J. & GAVRILOV, A. A. 1974 On the theory of self-similar degeneracy of homogeneous isotropic turbulence. *Sov. Phys. JETP* **38**, 399–402.

BATCHELOR, G. K. 1948 Energy decay and self-preserving correlation functions in isotropic turbulence. *Q. Appl. Maths* **6**, 97–116.

BATCHELOR, G. K. 1953 *The Theory of Homogeneous Turbulence*. Cambridge University Press.

https://doi.org/10.1017/jfm.2017.110 Published online by Cambridge University Press

BATCHELOR, G. K. & TOWNSEND, A. A. 1947 Decay of vorticity in isotropic turbulence. *Proc. R. Soc. Lond.* A **190**, 534–550.

BURATTINI, P., ANTONIA, R. A. & DANAILA, L. 2005*a* Similarity in the far field of a turbulent round jet. *Phys. Fluids* **17**, 025101–025115.

BURATTINI, P., LAVOIE, P. & ANTONIA, R. A. 2005*b* On the normalized dissipation energy rate. *Phys. Fluids* **17**, 98103.

DANAILA, L., ANSELMET, F., ZHOU, T. & ANTONIA, R. A. 1999 A generalization of Yaglom's equation which accounts for the large-scale forcing in heated decaying turbulence. *J. Fluid Mech.* **391**, 359–372.

DARISSE, A., LEMAY, J. & BENAISSA, A. 2015 Budgets of turbulent kinetic energy, Reynolds stresses, variance of temperature fluctuations and turbulent heat fluxes in a round jet. *J. Fluid Mech.* **774**, 95–142.

DJENIDI, L. & ANTONIA, R. A. 2014 Transport equation for the mean turbulent energy dissipation rate in low-R_λ grid turbulence. *J. Fluid Mech.* **747**, 288–315.

DJENIDI, L. & ANTONIA, R. A. 2015 A general self-preservation analysis for decaying homogeneous isotropic turbulence. *J. Fluid Mech.* **773**, 345–365.

DJENIDI, L., ANTONIA, R. A., LEFEUVRE, N. & LEMAY, J. 2016 Complete self-preservation on the axis of a turbulent round jet. *J. Fluid Mech.* **790**, 57–70.

DJENIDI, L., KAMRUZZAMAN, M. & ANTONIA, R. A. 2015 Power-law exponent in the transition period of decay in grid turbulence. *J. Fluid Mech.* **779**, 544–555.

DJENIDI, L., TARDU, S. F., ANTONIA, R. A. & DANAILA, L. 2014 Breakdown of Kolmogorov's first similarity hypothesis in grid turbulence. *J. Turbul.* **15**, 596–610.

DOERING, C. R. & FOIAS, C. 2002 Energy dissipation in body-forced turbulence. *J. Fluid Mech.* **467**, 289–306.

DONZIS, D. A., SREENIVASAN, K. R. & YEUNG, P. K. 2005 Scalar dissipation rate and dissipative anomaly in isotropic turbulence. *J. Fluid Mech.* **532**, 199–216.

GOMES-FERNANDES, R., GANAPATHISUBRAMANI, B. & VASSILICOS, J. C. 2012 Particle image velocimetry study of fractal-generated turbulence. *J. Fluid Mech.* **711**, 306–336.

HEARST, R. J. & LAVOIE, P. 2014 Decay of turbulence generated by a square-fractal-element grid. *J. Fluid Mech.* **741**, 567–584.

KANEDA, Y., ISHIHARA, T., YOKOKAWA, M., ITAKURA, K. & UNI, A. 2003 Energy dissipation rate and energy spectrum in high resolution direct numerical simulations of turbulence in a periodic box. *Phys. Fluids* **15**, L21–L24.

KOLMOGOROV, A. N. 1941*a* The locally structure of structure in incompressible viscous fluid for very large Reynolds number. *Dokl. Akad. Nauk SSSR* **30**, (see also *Proc. R. Soc. Lond.* A (1991), **434**, 9–13).

KOLMOGOROV, A. N. 1941*b* On degeneration of isotropic turbulence in an incompressible viscous liquid. *Dokl. Akad. Nauk SSSR* **31** (6), 538–541; (see also Selected works of A. N. Kolmogorov, in Mathematics and its applications (Soviet Series) vol. 25, pp 319–323).

KOLMOGOROV, A. N. 1962 A refinement of previous hypotheses concerning the local structure of turbulence in a viscous incompressible fluid at high Reynolds number. *J. Fluid Mech.* **13**, 82–85.

KROGSTAD, P.-Å. & DAVIDSON, P. A. 2011 Freely decaying, homogeneous turbulence generated by multi-scale grids. *J. Fluid Mech.* **680**, 417–434.

LEE, S. K., DJENIDI, L., ANTONIA, R. A. & DANAILA, L. 2013 On the destruction coefficients for slightly heated decaying grid turbulence. *Intl J. Heat Fluid Flow* **43**, 129–136.

LOHSE, D. 1994 Crossover from high to low Reynolds number turbulence. *Phys. Rev. Lett.* **73**, 3223–3226.

MAZELLIER, N. & VASSILICOS, J. C. 2010 Turbulence without Richardson–Kolmogorov cascade. *Phys. Fluids* **22**, 075101.

MCCOMB, W. D. 2014 *Homogeneous, Isotropic Turbulence, Phenomenology, Renormalization and Statistical Closures*. Oxford University Press.

MCCOMB, W. D., BERERA, A., SALEWSKI, M. & YOFFE, S. 2010 Taylor's (1935) dissipation surrogate reinterpreted. *Phys. Fluids* **22**, 061704.

https://doi.org/10.1017/jfm.2017.110 Published online by Cambridge University Press

McComb, W. D., Berera, A., Yoffe, S. R. & Linkmann, M. F. 2015 Energy transfer and dissipation in forced isotropic turbulence. *Phys. Rev.* E **91**, 043013.

Meldi, M. & Sagaut, P. 2013 Further insights into self-similarity and self-preservation in freely decaying isotropic turbulence. *J. Turbul.* **14**, 24–53.

Monin, A. S. & Yaglom, A. M. 2007 *Statistical Fluid Mechanics: Mechanics of Turbulence*, vol. II (Republication). Dover.

Pearson, B. R. & Antonia, R. A. 2001 Reynolds-number dependence of turbulent velocity and pressure increments. *J. Fluid Mech.* **444**, 343–382.

Pearson, B. R., Krogstad, P.-Å. & van de Water, W. 2002 Measurements of the turbulent energy dissipation rate. *Phys. Fluids* **14**, 1288–1290.

Sinhuber, M., Bodenschatz, E. & Bewley, G. P. 2015 Decay of turbulence at high Reynolds numbers. *Phy. Rev. Lett.* **114**, 034501.

Sreenivasan, K. 1984 On the scaling of the turbulence energy dissipation rate. *Phys. Fluids* **27**, 1048–1058.

Sreenivasan, K. 1998 An update on the energy dissipation rate in isotropic turbulence. *Phys. Fluids* **10**, 528–529.

Succi, S. 2001 The lattice Boltzmann equation for fluid dynamics and beyond. In *Numerical Mathematics and Scientific Computation*, Oxford University Press.

Tang, S. L., Antonia, R. A., Djenidi, L., Abe, H., Zhou., T., Danaila, L. & Zhou, Y. 2015*a* Transport equation for the meant turbulent energy dissipation rate on the centreline of a fully developed channel flow. *J. Fluid Mech.* **777**, 151–177.

Tang, S. L., Antonia, R. A., Djenidi, L. & Zhou, Y. 2015*b* Complete self-preservation along the axis of a circular cylinder far wake. *J. Fluid Mech.* **786**, 253–274.

Tang, S. L., Antonia, R. A., Djenidi, L. & Zhou, Y. 2015*c* Transport equation for the meant turbulent energy dissipation rate in the far-wake of a circular cylinder. *J. Fluid Mech.* **784**, 109–129.

Taylor, G. I. 1935 Statistical theory of turbulence. *Proc. R. Soc. Lond.* A **141**, 421–444.

Tennekes, I. & Lumley, J. 1972 *A First Course in Turbulence*. MIT Press.

Thiesset, F., Antonia, R. A. & Djenidi, L. 2014 Consequences of self-preservation on the axis of a turbulent round jet. *J. Fluid Mech.* **748**, R2.

Townsend, A. A. 1956 *The Structure of Turbulent Shear Flow*. Cambridge University Press.

Townsend, A. A. 1976 *The Structure of Turbulent Shear Flow*. Cambridge University Press.

Vassilicos, J. C. 2015 Dissipation in turbulent flows. *Annu. Rev. Fluid Mech.* **47**, 95–114.

Wang, L. P., Chen, S., Brasseur, J. G. & Wyngaard, J. C. 1996 Examination of hypotheses in the kolmogorov refined turbulence theory through high-resolution simulations. Part I. Velocity field. *J. Fluid Mech.* **309**, 113–156.

Yeung, P. K., Donzis, D. A. & Sreenivasan, K. R. 2012 Dissipation, enstrophy and pressure statistics in turbulence simulations at high Reynolds numbers. *J. Fluid Mech.* **700**, 5–15.

Zhou, T., Pearson, B. R. & Antonia, R. A. 2001 Comparison between temporal and spatial transverse velocity increments in a turbulent plane jet. *Fluid Dyn. Res.* **28**, 127–138.

https://doi.org/10.1017/jfm.2017.110 Published online by Cambridge University Press